Dynamics and Self-Healing of Layer-by-Layer Hydrogen-Bonded Films of Linear Synthetic Polyphenols

Raman Hlushko[1], John F. Ankner[2], and Svetlana Sukhishvili[1]*

[1]*Department of Materials Science and Engineering, Texas A&M University*

College Station, Texas 77843, USA

[2]*Spallation Neutron Source, Oak Ridge National Laboratory, Oak Ridge, Tennessee 37831, USA*

Abstract

This work explores the dynamics of hydrogen-bonded layer-by-layer (LbL) films of linear synthetic polyphenols (*l*PPhs) with different backbone and pendant group structures. The polymers feature repeat units with catechol-like or gallol-like polyphenol rings, namely poly(3,4-dihydroxybenzyl methacrylamide) (P2HMA), poly(3,4-dihydroxybenzyl acrylamide) (P2HAA), poly(3,4,5-trihydroxybenzyl acrylamide) (P3HAA) and poly(3,4,5-trihydroxybenzyl methacrylamide) (P3HMA), and were assembled with linear poly(ethylene oxide) (PEO). The structure of the *l*PPhs has a major effect on the diffusivity of LbL films, and chain dynamics is asymmetric for *l*PPh- and PEO-terminated films during film construction. Specifically, diffusivity of polyphenols in the direction perpendicular to the substrate varied from values below ~10^{-17} $cm^2\ s^{-1}$ to ~10^{-14} $cm^2\ s^{-1}$ for *l*PPhs of the P2 and P3 families, as assessed by *in situ* ellipsometry during film assembly. The uptake of the most diffusive P3HMA follows the subdiffusive behavior with the anomalous diffusion exponent $\beta \approx 0.3$. Similarly, large differences in film dynamics were revealed by neutron reflectometry, which detected fast penetration of deuterated PEO (*d*PEO) through the entire film with a diffusion coefficient > 10^{-12} $cm^2\ s^{-1}$ through P3HMA/PEO films, but accumulation of *d*PEO only at the film surface for all other *l*PPh/PEO systems during the first 10

minutes of the experiment. The observed trends in film dynamics were consistent with strongly exponential growth of P3HMA/PEO films, and largely linear deposition of non-diffusive P2/PEO systems. Finally, the self-healing behavior of *l*PPh/PEO films in an aqueous environment was quantified by *in situ* AFM experiments, which revealed robust self-healing of P3/PEO films occurring on a time scale of minutes, and an absence of film healing for P2/PEO films.

Introduction

Layer-by-layer (LbL) deposition of polymers at surfaces has become a powerful tool for assembly of functional coatings for a variety of applications.[1] For example, LbL coatings can be created to enhance tissue regeneration,[2,3] provide hemocompatibility, add antibacterial and antioxidant activity to biomedical devices,[3] or to control localized delivery of bioactive molecules.[4-6] Among various intermolecular forces that control LbL assembly, such as electrostatic,[7,8] metal-ligand coordination,[9] or hydrophobic interactions,[10] hydrogen bonding is unique in its ability to assemble neutral molecules and so to incorporate antioxidant polyphenol molecules within surface coatings.[11-16] While earlier hydrogen-bonded films were mostly based on assembly of poly(carboxylic acids) which assembled with neutral polybases at acidic pH and dissociated in neutral and basic environments, [14,15,17-19] more recent studies have focused on assembly of a neutral polyphenol molecule – tannic acid (TA), which yields robust films stable over a wide range of conditions, including physiological ones.[20] Inclusion of polyphenols within LbL films opens a way for combining nontoxicity with polyphenol-provided antioxidant and radical-scavenging activity. For example, TA-based assemblies were used for encapsulation of living cells [21,22] and construction of nontoxic capsules that can modulate immune response[23-25].

The fundamental principles of hydrogen-bonded LbL assemblies and their structure-property relations are less well understood, however, than are those of their electrostatically

assembled counterparts. For electrostatically assembled LbL films, it is well established that film structure and polymer chain diffusivity are dependent on the strength of interpolymer ionic pairing,[6,26-28] polymer molecular weight,[29,30] chain rigidity,[31] and that these parameters can be controlled by film processing conditions, such as solution pH,[32] salt concentration,[33] temperature,[34] and assembly time. [35] For hydrogen-bonded films, correlations between the strength of hydrogen-bonding and the film growth regime (linear *vs*. exponential) have been established. For example, strongly bound polyvinylpyrrolidone/poly(methacrylic acid) (PVP/PMAA) films deposited linearly,[36] while weakly associated poly(ethylene oxide)/PMAA (PEO/PMAA) films exhibited exponential growth.[37] These growth regimes have been correlated with the degree of polymer chain intermixing within hydrogen-bonded films as determined in neutron reflectometry (NR) experiments.[38] Unlike electrostatic systems, hydrogen-bonded assemblies typically do not involve charge pairing, and deposition does not require charge balance within the films, exhibit osmotic effects associated with counterions, or be limited by the long-range repulsion that terminates deposition of polyelectrolyte chains. Instead, polymer chains are deposited through saturation of hydrogen-bonded sites within the film. Distinct from ionic pairing, hydrogen-bonding sites are only weakly sensitive to salt concentration.[19] Instead, the strength of hydrogen bonding can be modulated by an addition of small molecules which act as hydrogen bonding competitors.[36] Similar to salt ions in electrostatic LbL films, such competitors weaken polymer-polymer interactions and can strongly affect film growth mode or even destroy LbL assemblies.[36]

It is usually assumed that hydrogen-bonding interactions are weaker than electrostatic coupling and lead to reversible, dynamic assemblies.[39,40] However, hydrogen bonding is strengthened by hydrophobic interactions in aqueous media,[41] and a wide range of layer interdiffusion modes are observed in hydrogen-bonded LbL films.[38,42] In electrostatic

polyelectrolyte assemblies, chain dynamics has been explored by a variety of techniques. Wide-line ^{2}H NMR spectroscopy revealed a dependence of chain mobility on the nature of the capping layer[43]. Numerous studies of the lateral diffusivity of polymer chains have also been performed for different electrostatically assembled LbL films using fluorescence recovery after photobleaching (FRAP)[17,31,33,42]. Simultaneously, salt-triggered layer intermixing and chain diffusion in the direction perpendicular to the substrate was explored using neutron reflectometry (NR), [33,44-46] revealing an anisotropy of chain dynamics in salt solutions of linearly growing polyelectrolyte multilayers.[47] Another technique to assess the dynamics of polymer assemblies is based on monitoring the evolution of surface morphology by atomic force microscopy (AFM)[48,49]. Smoothening of the surface of electrostatically assembled films was observed due to the movement of polyelectrolytes from "peaks" to "valleys" during films annealing in a salt solution, and surface (inter)diffusion coefficients of 10^{-15}–10^{-14} cm^2 s^{-1} were estimated for these systems.[48] However, these studies have not up to now been applied to hydrogen bonded films. Studies of dynamics in hydrogen-bonded systems so far have been limited to the application of wide-line ^{2}H NMR spectroscopy to films composed of weak poly(carboxylic acids) with neutral polymer acceptors, such as PVP and PEO.[50]

In this work, we use a combination of *in situ* ellipsometry, NR, and AFM techniques to explore the dynamics of polymer chains and self-healing in hydrogen-bonded assemblies. These studies are performed with linear synthetic polyphenol polymers rather than with the previously studied films of poly(carboxylic acids). A family of synthetic polyphenols with two or three polyphenol groups in the benzene ring has been synthesized by our group and shown to exhibit antioxidant properties.[51,52] We demonstrated that the structure of the polyphenol rings has a strong effect on the film growth regime, film internal structure, and the ability of these assemblies to

scavenge radicals.[53] In this work, we aim to understand the underlying dynamics driving these behaviors. Using NR to track infusion of deuterated PEO chains into linear and exponential hydrogen-bonded LbL films, *in situ* ellipsometry to monitor kinetics of mass deposition during film construction, and AFM to track healing of tip-indented films upon exposure to water, we have uncovered differences in chain diffusivity between film components during film construction, and correlate these with film growth mode and the structure of the polyphenol ring in hydrogen-bonded linear polymers.

Materials and methods

Branched polyethylene imine (BPEI) with number-average molecular weight (M_n) of 60,000 g/mol, ethanol, sodium hydroxide, hydrochloric acid, sodium hydrogen phosphate, and potassium persulfate were purchased from Sigma-Aldrich and used as received. Polyethylene oxide (PEO) with M_n 95,000 g/mol, polydispersity index (PDI) of 1.08, and deuterated poly(ethylene oxide-*d*4) (*d*PEO) with M_n 93,000 g/mol and PDI 1.07 were purchased from Polymer Source, Inc. Linear synthetic polyphenols (*l*PPh) with two and three hydroxyl groups in the benzene ring and methacrylamide or acrylamide backbones were synthesized using reversible addition–fragmentation chain transfer (RAFT) polymerization. Polymers with a methacrylamide backbone, *i.e.* poly(3,4-dihydroxybenzyl methacrylamide) (P2HMA, M_n 35,900 g/mol, PDI 1.20) and poly(3,4,5-trihydroxybenzyl methacrylamide) (P3HMA, M_n 43,400 g/mol, PDI 1.45), were prepared as described in our previous publication.[52] At the same time, synthesis and characterization of acrylamide-backbone polymers, *i.e.* poly(3,4-dihydroxybenzyl acrylamide) (P2HAA, M_n 36,400 g/mol, PDI 1.17) and poly(3,4,5-trihydroxybenzyl acrylamide) (P3HAA, M_n 42,300 g/mol, PDI 1.20), was performed in this work for the first time and is described in the Supporting Information (shown schematically in Figure S1).

Film Deposition. Silicon wafers (0.5-mm-thick, undoped) used for ellipsometric studies of LbL film deposition and silicon pucks (<111>, 50 mm-diameter, 4.0 mm-thick) used for neutron reflectometry studies of polymer-chain diffusion were both obtained from the Institute of Electronic Materials Technology, Poland. Prior to LbL film deposition, the substrates were cleaned by UV radiation and concentrated sulfuric acid and primed with a monolayer of BPEI, which was adsorbed from a 0.2 mg/mL solution at pH 9 for 20 min as described in our previous publication.[54] Construction of *l*PPh/PEO films was then performed (starting from deposition of *l*PPh) using a sequential exposure of the substrates in 0.2 mg/mL solutions of *l*PPh and PEO in ethanol or water, respectively, and application of two rinsing cycles in between the polymer deposition steps. The rinsing steps after deposition of *l*PPh were performed in ethanol first and then in an ethanol/water (1:1 by volume) mixture, while PEO-capped films were first rinsed with water and then with a 1:1 v/v ethanol/water mixture. For studies of film growth modes by ellipsometry and neutron reflectometry, deposition was performed manually using a 5-min immersion in each polymer solution, followed by careful drying of the films in a gentle flow of nitrogen gas after each deposition cycle prior to analysis.

For studies of healing in an aqueous environment using *in situ* AFM, *l*PPh/PEO films with ~ 400-nm dry thickness were deposited using a Riegler & Kirstein GmbH DR-3 table-top robotic system at a 0.5 cm/s dipping and withdrawal rate.

Spectroscopic Ellipsometry. The thicknesses of LbL films deposited on silicon wafers were determined using a variable angle spectroscopic ellipsometer (M-2000, J.A. Woollam Co., Inc.) equipped with a temperature-controlled liquid cell. Dry measurements were performed at four incidence angles: 45, 55, 65, and 75°. A single incident angle of 75° was used in liquid-cell measurements due to cell geometry. The thicknesses of the native oxide layers on the silicon wafers

were measured prior to depositing the LbL films. The data for dry LbL films were fitted using a three-stack model. The first two stacks were the silicon substrate and the oxide layer. The third stack was characterized as a Cauchy material of thickness *d*. The wavelength dependence of the refractive index was modeled by $n(\lambda) = A + B/\lambda^2 + C/\lambda^4$, where λ is wavelength and A, B, and C are fitted coefficients. [55]

For studies of polymer chain uptake using *in-situ* ellipsometry, *l*PPh/PEO films were first placed in a liquid ellipsometry cell supplied by J.A. Woollam Co. The cell was then filled with a solvent (water for PEO-top-layer films, ethanol for *l*PPh-top films). The film was immersed for 30 min in the solvent. Then the cell was filled with 0.2 mg/mL polymer solution in the corresponding solvent (water for PEO or ethanol for *l*PPh) and the wet thickness data were collected. After exposure to the polymer solution, the film in the cell was rinsed three times by 25 mL of the corresponding solvent.

For the swollen films, a four-stack model was used, wherein the solvent was considered as the fourth stack, characterized as a semi-infinite transparent Cauchy medium. The dependence of refractive index on wavelength was determined prior to each measurement using a bare silicon wafer installed in the liquid cell. The four variables A, B, C, and thickness d were fitted simultaneously.

Atomic Force Microscopy (AFM) studies were performed using a Bruker Dimension Icon AFM instrument in ScanAsyst mode using a ScanAsyst Fluid+ probe (k = 0.7 N/m, f=150 kHz, R=2.0 nm). All samples were immersed in DI water for 60 min prior to measurement to allow for equilibrated water uptake. Indentation was then induced with the tip in contact mode by applying a force of 2-20 nN for 5 min. After that, the substrate containing the indented region was scanned continuously (scanned area 2×2 μm^2, resolution 256 points) in the ScanAsyst mode (an advanced

version of the PeakForce tapping mode) using the same tip. The images were analyzed using the ProfilmOnline tool.

Neutron reflectometry measurements were performed at the Spallation Neutron Source Liquids Reflectometer (SNS-LR) at the Oak Ridge National Laboratory (ORNL). The reflectivity data were collected using a sequence of 3.4-Å-wide continuous wavelength bands (selected from 2.55 Å < λ < 16.70 Å) and incident angles (ranging over 0.6° < θ < 2.34°). Using these settings, the momentum transfer, $Q = (4\pi \sin\theta/\lambda)$, was varied over a range of 0.008 $Å^{-1} < Q < 0.20$ $Å^{-1}$. Reflectivity curves were assembled by combining seven different wavelength and angle data sets together, maintaining a constant relative instrumental resolution of $\delta Q/Q = \delta\theta/\theta = 0.023$ by varying the incident-beam apertures.

Neutron scattering densities within hydrogenated and deuterated stacks were averaged, each stack exhibiting its characteristic thickness, scattering density, and interlayer roughness. The characteristic parameters of the films were adjusted until the reflectivity curve was best fitted (minimized χ^2), as described in the Supporting Information.

Results and Discussion

Figure 1A illustrates deposition of hydrogen-bonded LbL films of linear polyphenol polymers (*l*PPhs) with PEO on the surface of BPEI-primed silicon wafers. The formation of hydrogen bonds between *l*PPh and PEO has been observed in our previous work by spectroscopic changes in a broad O–H stretching band of *l*PPhs.[53] The four linear polyphenols used for film construction had either catechol-like structure with two hydroxyl groups (such as in P2HMA and P2HAA) or gallol-like structure with three hydroxyl groups in the benzene ring (such as in P3HMA and P3HAA), and either an acrylate or methacrylate polymer backbone. All *l*PPhs polymers,

synthesized by RAFT polymerization had similar degrees of polymerization (DPs) of 190 ± 12 and polydispersity indices (PDIs) of 1.17 – 1.45. Synthesis of P2HMA and P3HMA is described in our previous work,[52] while procedures for synthesis and characterization of a new pair of linear polyphenols with an acrylic backbone (*i.e.* P2HAA and P3HAA) can be found in the Supporting Information for this manuscript.

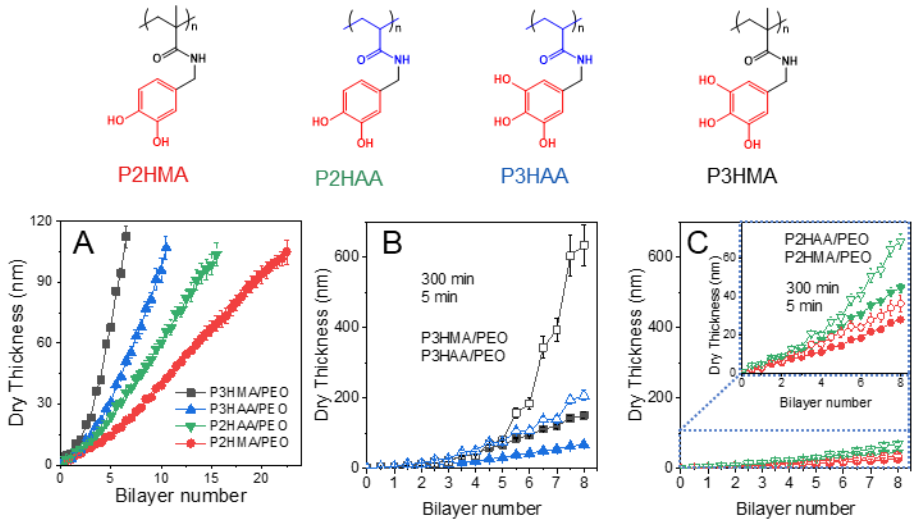

Figure 1. Dry thickness measured by spectroscopic ellipsometry during sequential deposition of *l*PPh/PEO films from 0.2 mg/ml polymer solutions using a 5 min per layer deposition time (A), and a comparison of dry film thicknesses measured using deposition time of 5 min (solid symbols) and 300 min per layer (open symbols) for P3/PEO systems (B) and P2/PEO systems (C).

Figure 1A shows that the fastest increase in thickness occurs for the P3HMA/PEO system, with film thickness reaching 112 nm after as few as 6.5 bilayer deposition cycles, and the slowest thickness increase is observed in the P2HMA/PEO system, with a total thickness of only 105 nm reached after deposition of as many as 22.5 bilayers. These differences in film growth are rationalized by a greater tendency of the P3HMA polymer to self-association through hydrogen bonding between gallol polymer units as discussed in our prior publication.[53] Note that the

difference in film growth mode for polymers with catechol-like and gallol-like units was smaller for acrylate polymer backbone polymers than it was for methacrylate backbones (acrylates P3HAA and P2HAA vs. methacrylates P3HMA and P2HMA), suggesting a possible effect of backbone hydrophobicity on self-association of polyphenol units. To further study differences in the mechanism of *l*PPh/PEO film growth brought about by the chemistry of polyphenol units, we probed the diffusivity of polymers and its role in the accumulation of film mass. To that end, the deposition time was increased from 5 min to 300 min per layer. Figure 1B shows that the effect of an increase in deposition time on dry film thickness was drastically different for P3HMA/PEO and P2HMA/PEO films, in agreement with the diffusive character of exponential vs. the non-diffusive character of linearly deposited films. Also note that while the gallol-containing systems demonstrated exponential growth in the beginning (up to 5-6 bilayers for P3HMA/PEO), film growth became linear for larger numbers of bilayers, wherein the time required for polyphenol molecules to diffuse through the entire film exceeded the layer deposition time. Time-induced mass increase was the largest for the most exponential P3HMA/PEO film, and smallest for the P2HMA/PEO system, with the P3HAA/PEO and P2HAA/PEO systems exhibiting an intermediate rate of film thickness accumulation (Figure 1B). Interestingly, the long-term uptake of *l*PPh and PEO was highly asymmetric for exponential P3HMA/PEO films. P3HMA contributes most of the film mass (half-integer bilayer numbers in Figure 1B), reaching ~200 nm per layer during deposition of a 7-bilayer film, while the amount of PEO added to the film did not exceed 10-20 nm per layer. The larger amount of P3HMA is consistent with self-association of P3HMA polyphenol groups, which reduced the density of hydrogen-bonding sites of this polymer available to PEO.

To further understand this asymmetry in deposition of *l*PPh and PEO components during LbL assembly, kinetic experiments on each layer deposition were performed by *in situ* ellipsometry and complemented by dry thickness measurements of mass deposited upon saturation. These experiments utilized films with matched dry thicknesses of 100±5 nm followed by 5-min deposition cycles and capped with *l*PPh or PEO for further *in situ* PEO or *l*PPh deposition, respectively. The films were then pre-swollen in water or ethanol for 30 min (time t = 0 in Figures 2A and 2B), then PEO or *l*PPh solution was added to the *in situ* ellipsometry cell. Addition of 0.2 mg/ml PEO (Figure 2A) or *l*PPh solution (Figure 2B) resulted in changes in wet film thickness associated with incorporation of polymers within the films. For all films, adsorption of PEO was fast and levelled off after about 10 min. The amount of PEO adsorbed on or absorbed by the films after 20 minutes (determined by the dry thickness increase measured by ellipsometry) systematically increased from 1.5 nm to 1.7 nm, 4.8 and 10.3 nm for P2HMA/PEO, P2HAA/PEO, P3HAA/PEO and P3HMA/PEO films, respectively. Regardless of the total mass adsorbed, PEO deposition for all the films was fast (Figure 2A). At the same time, large differences in the rate of increase of wet thickness were revealed for the different *l*PPhs: while film wet thicknesses equilibrated after ~5 minutes of exposure to P2HMA, other polyphenols showed ongoing long-term absorption within the films, which likely indicated slow penetration of the polyphenols into the LbL films (Figure 2B). The dry thickness increase due to uptake of *l*PPhs was 3.3 nm, 6.7 nm, 11.1 nm and 35.3 nm for P2HMA, P2HAA, P3HAA and P3HMA, respectively. Figure 2C shows that for uptake of PEO within *l*PPh-capped films, film swelling ratios (measured as the ratio of wet to dry ellipsometric thickness) varied between the different *l*PPh systems but did not change significantly after PEO uptake. Specifically, for the P2HMA/PEO film, the swelling ratios were 1.03±0.08 and 1.10±0.10 before and after 20-min PEO deposition, respectively. While the other

*l*PPh/PEO films were more swollen, no significant changes were detected during PEO deposition. The highest swelling ratio was observed for P3HMA/PEO system, which featured the highest rate of exponential growth. For uptake of *l*PPh within PEO-capped films, while changes in wet film thickness for most of the *l*PPh/PEO films occurred over long times (Figure 2B), and except for the P2HMA/PEO film whose swelling did not change before and after a 300-min P2HMA deposition, swelling ratios of the other films slightly increased after *l*PPh deposition (Figure 2D). The refractive indices (RIs) obtained by fitting ellipsometry data for the wet films using the Cauchy model with a constant value of A[55] gave good fits with low mean square error values, suggesting that the refractive indices (RIs) of the swollen films can be assumed constant during polymer uptake. However, RIs were lower for P2/PEO films than those for P3/PEO films (1.487 and 1.485 for P2HMA/PEO, 1.493 and 1.491 for P2HAA/PEO, 1.510 and 1.513 for P3HAA/PEO, and 1.517 and 1.515 for P3HMA/PEO films during PEO and *l*PPh uptake, respectively (data not shown). The higher refractive indices of P3/PEO films, observed for the swollen films despite their higher solvent content (RI of water is 1.333 and RI of ethanol is 1.362) is explained by a larger fraction of P3 polymers in *l*PPh/PEO films, also seen in the data in Figure 1, and indicates that the RIs of *l*PPhs (which could not be directly determined in this study) are higher than that of PEO (RI 1.46).[56] In the experiments shown in Figure 2, the greatest degree of film swelling caused by a long-term uptake of a polymer, observed for uptake of P3HMA within P3HMA/PEO films, was moderate (1.67±0.11). This observation is drastically different from our earlier study of electrostatic exponential LbL films, which instead demonstrated dramatic increases in film swelling (from 2.4 to 3.8) upon invasion of polyelectrolyte chains from solution.[57] The two cases are clearly distinct because of the absence of electrostatic charge regulation and the osmotic pressure of counterions as factors controlling swelling of hydrogen-bonded films.

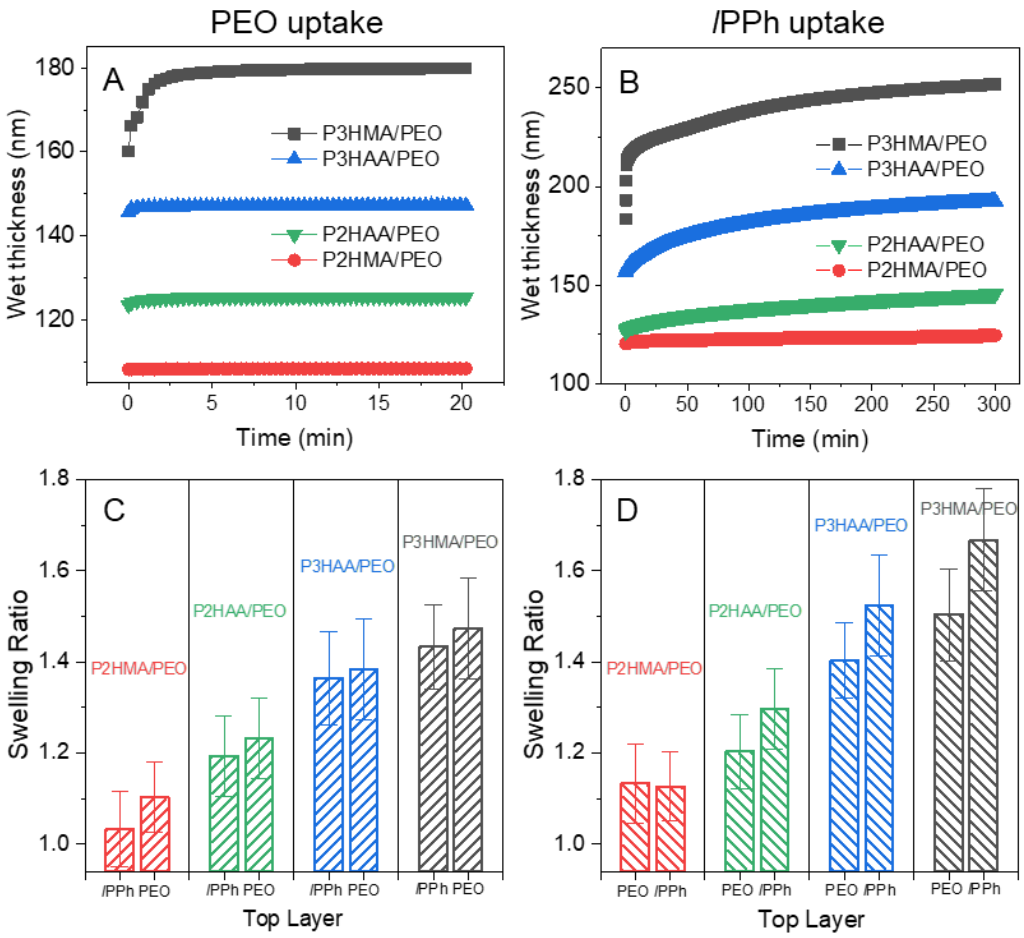

Figure 2. *In situ* spectroscopic ellipsometry measurements of the uptake of PEO or *l*PPhs from 0.2 mg/ml aqueous or ethanol solutions (A and B, respectively) by ~100-nm *l*PPh/PEO films constructed using 5-min per layer deposition time. Swelling ratios of *l*PPh/PEO films constructed using 5-min per layer deposition time in water or ethanol (C and D, respectively) before and after 20-min exposure to 0.2 mg/ml PEO solutions (C), or before and after 300-min exposure to 0.2 mg/ml *l*PPh solutions (D). For measurements of swelling ratios, films were rinsed by a solvent after completion of polymer adsorption.

While at short times (up to 5 min) the binding of polymers in LbL is likely limited by solution flux, longer interaction times allow for rearrangement of assembled polymer chains and diffusion of polymer chains into the bulk of the films. The kinetics of *l*PPh uptake shown in Figure 2B, enables estimation of rates and diffusion coefficients for the penetration of polyphenol chains into the film. However, in the case of P2HMA/PEO, the diffusion coefficient was lower than 10^{-17} cm^2/s and was not quantified because of the uncertainty associated with the measurement of such slow diffusion over a short time. For P3HAA/PEO and P2HAA/PEO films, the polymer diffusivity within the bulk of the film was roughly estimated assuming a Fickian diffusion model: $Dt = q^2H^2/4$, where D is the diffusion coefficient of deposited polymer chains through the wet polymer film, and q is the normalized mass uptake, calculated from measurements of wet film thickness as $(l_t - l_0)/(l_\infty - l_0)$, where l_0, l_t, and l_∞ are the initial, effective (at time t), and equilibrium thicknesses of dry films, t is the exposure time to a polyphenol solution, and H is the film wet thickness at time t as detected with spectroscopic ellipsometry. These estimates yield diffusion coefficients D for penetration of polyphenols through *l*PPh/PEO films decreasing from $(1.6 \pm 0.2) \times 10^{-16}$ cm^2/s for P3HAA/PEO to $(4.9 \pm 0.5) \times 10^{-17}$ cm^2/s for P2HAA/PEO films, in agreement with the transition from a more exponential to a more linear growth mode for these films. In contrast, for the most diffusive P3HMA/PEO system, the uptake of P3HMA did not follow the Fickian diffusion model. Instead, the instantaneous diffusion coefficient varied with time, following the anomalous diffusion model with the mean square displacement scaling with time as $\langle r^2(t) \rangle \sim t^{\beta}$, where $\beta < 1$.[58-60] The anomalous diffusion was previously found for lateral diffusion of polymers within polyelectrolyte multilayers in salt solutions.[61] Here, for hydrogen-bonded films, fitting the instantaneous value of the diffusion coefficient between 5 and 300 min revealed a monotonous decrease of D from $(1.8 \pm 0.1) \times 10^{-14}$ cm^2/s to $(8.6 \pm 0.1) \times 10^{-16}$ cm^2/s, with the

scaling exponent $\beta \approx 0.3$ (Figure S2). This behavior reflects subdiffusive motion of P3HMA chains within bulk of the film, indicating inhomogeneous environment within the film as a function of depth, that can be also affected by self-association of P3HMA. It should be also noted that while the diffusivity estimates are consistent with differences in film growth modes observed in *l*PPh/PEO films, the ellipsometry technique used for these measurements is unable to directly assess diffusivity of polymer chains. Moreover, asymmetry in the mass deposition of *l*PPh and PEO within the film poses a question of whether the PEO deposited within the film in much smaller amounts than *l*PPh can diffuse within the film during deposition, and thus support self-healing of these films in an aqueous environment.

To explore the diffusivity of PEO chains within *l*PPh/PEO films, we have used neutron reflectometry. In this technique, we took advantage of the contrast provided by deuterated polyethylene glycol (poly(ethylene glycol-d_4), *d*PEO) whose molecular weight and polydispersity (M_n 93,000 g/mol, PDI 1.07) were closely matched to those of the hydrogenated PEO chains (*h*PEO, M_n 95,000 g/mol, PDI 1.08). Neutron reflectometry has been traditionally used to study the internal structure of LbL films after their assembly, and has been applied to both electrostatically assembled[57] and hydrogen-bonded films[53]. In this paper, we instead designed an experiment in which pre-assembled hydrogenated films were exposed to a solution of *d*PEO for different time intervals and the diffusivity of film-invading chains was then accessed by measurements of the dry films. We used a similar approach previously to study chain diffusivity within electrostatically assembled films.[57] In this work, hydrogenated *l*PPh/PEO films were deposited using a BPEI priming layer and a 5-min per layer deposition time to achieve a total thickness of ~100-110 nm. Maintaining constant thickness required assembly of a different number of layers for different *l*PPh/PEO pairs (Figure 1A). Specifically, the film thicknesses of 105.0 ±

5.9 nm, 103.8 ± 5.4 nm, 107.1 ± 5.7 nm, and 112.4 ± 5.1 nm were achieved with 22.5-bilayer 15.5-bilayer, 10.5-bilayer, and 6.5-bilayer films of P2HMA/PEO, P2HAA/PEO, P3HAA/PEO, and P3HMA/PEO films, respectively. For these experiments, films featuring *l*PPh as a capping layer were exposed to a 0.2 mg/mL aqueous solution of *d*PEO for a sequence of time intervals to allow for observation of diffusion of the deuterated marker polymer through the hydrogenated film. The model used for the dry films included a silicon oxide layer, a BPEI priming layer, an underlying *d*PEO-poor layer (H-stack), and a surface layer (D-stack) whose scattering-length-density (SLD) increases after exposure to the *d*PEO solution. The SLD values of hydrogenated and deuterated stacks (H-stack and D-stack, respectively) were determined by fitting the reflectivity data.

One parameter that accessible to both neutron reflectometry and ellipsometry is the volume fraction of PEO (f_{PEO}) in *l*PPh/PEO films, and we aimed to check the consistency of f_{PEO} values obtained by the two techniques. In neutron reflectometry, this parameter was determined for the hydrogenated films before their exposure to *d*PEO, and yielded values of 0.34 ± 0.06, 0.30 ± 0.05, 0.27 ± 0.06, and 0.24 ± 0.07 for P2HMA/PEO, P2HAA/PEO, P3HAA/PEO, and P3HMA/PEO films, respectively, with corresponding densities for these films of 1.36 ± 0.07 g/cm^{-3}, 1.37 ± 0.06 g/cm^{-3}, 1.27 ± 0.07 g/cm^{-3} and 1.21 ± 0.07 g/cm^{-3} (Tables S2, S7, S12, S17). These data, together with the known density of amorphous PEO of 1.13 g/cm^{-3},[62] allowed us to determine densities of individual *l*PPh components. These values were systematically higher for P2 polymers as compared to P3 *l*PPhs, *i. e.* 1.40 g/cm^{-3} *vs.* 1.24 g/cm^{-3} for P2HMA *vs*. P3HMA, and 1.45 g/cm^{-3} *vs.* 1.31 g/cm^{-3} for P2HAA *vs*. P3HAA, respectively, probably reflecting tighter packing of linearly deposited P2 polymers within the films. When the calculated *l*PPh densities were used to determine ratios f_{PEO} from the average changes in dry ellipsometric thicknesses after addition of PEO or *l*PPh (Figure 1A), f_{PEO} values of 0.33 ± 0.16, 0.28 ± 0.14, 0.27 ± 0.11, and 0.24 ± 0.04 were found for

P2HMA/PEO, P2HAA/PEO, P3HAA/PEO, and P3HMA/PEO films, respectively. These values are in good agreement with the neutron reflectometry data and indicate the consistency of our analysis using the two techniques.

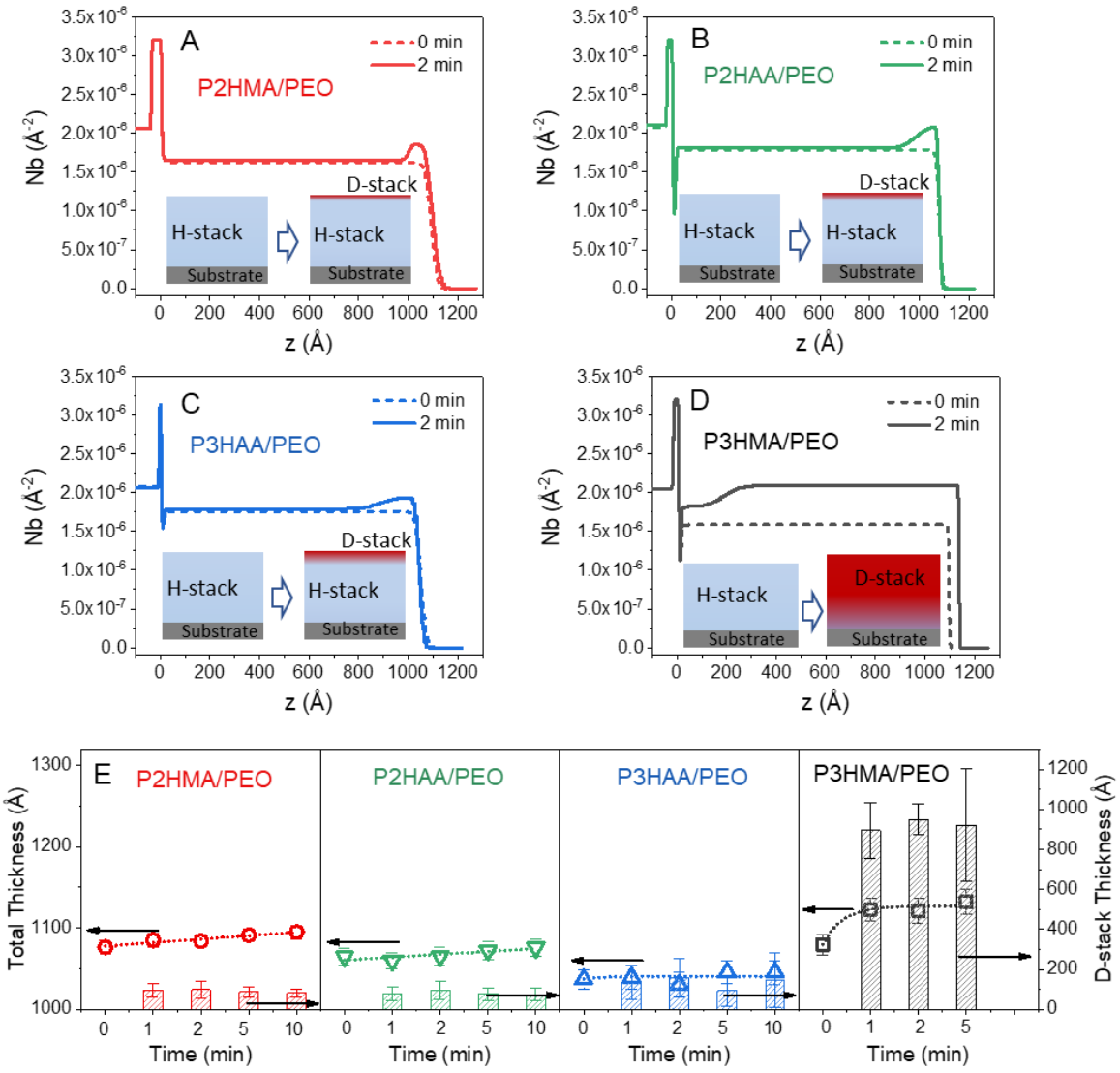

Figure 3. Scattering length density profiles (A-D) of hydrogenated *l*PPh/PEO films before (dashed lines) and after (solid lines) a 2-min exposure to a 0.2 mg/mL *d*PEO aqueous solution for 22-bilayer P2HMA/PEO (A), 15-bilayer P2HAA/PEO (B), 11-bilayer P3HAA/PEO (C), and 6-bilayer P3HMA/PEO (D) films, as well as changes in the total film thickness (symbols) and

thickness of the *d*PEO-rich surface layer (bars) upon exposure of *l*PPh/PEO films to 0.2 mg/mL *d*PEO aqueous solutions for different times (E). All films were dried prior to measurement.

Figure 3 A-D shows neutron reflectivity data, SLD profiles of different *l*PPh/PEO films upon exposure to *d*PEO solution, as well as schematic representations of the uptake of *d*PEO by the films. Figure 3E summarizes the results of the neutron reflectometry studies. The construction of the neutron reflectivity models and definitions of fitted parameters may be found in the Supporting Information. The linearly growing P2HMA/PEO film formed a diffuse *d*PEO-infused layer (the concentration of *d*PEO, *d*PEO/PEO, f_d^D = 0.12±0.06, see Eqn. S4) of dry thickness 8.5±3.3 nm at the film surface after 1-min exposure to a 0.2 mg/mL *d*PEO solution. Further exposure of this film to *d*PEO did not significantly change the SLD profile. These data demonstrate that *d*PEO does not penetrate deeply into the P2HMA/PEO hydrogenated matrix, but rather accumulates at the film surface through diffusion from solution, in agreement with the ellipsometry data for uptake of hydrogenated PEO in Figure 2A. Similar results were observed for adsorption of *d*PEO onto the P2HAA/PEO hydrogenated film (Figure 3E), *i.e*. thickness of the *d*PEO-infused (f_d^D = 0.13±0.05) layers remained constant at 7.1±3.4 nm for all *d*PEO adsorption times of 1-10 min, suggesting that similarly to the P2HMA/PEO system, *d*PEO accumulated at the surface of the P2HAA/PEO hydrogenated matrix.

In contrast, the gallol-based P3/PEO films demonstrated different trends for the uptake of deuterated PEO chains. As seen in Figure 3E, the interface between H-stacks and D-stacks was still located largely within the top region of the film for the P3HAA/PEO system, showing an intermediate behavior between surface accumulation and bulk penetration. However, *d*PEO penetrated throughout the film for P3HMA/PEO. Specifically, for the P3HAA/PEO, the

concentration of *d*PEO (*d*PEO/PEO, f_d^D = 0.10±0.04) was similar, and thickness of the D-stack film (d^D = 15.4±11.3 nm) was about twice larger than seen for P2/PEO, suggesting a more diffusive character. Finally, for the most exponential P3HMA/PEO system, D-stack (f_d^D = 0.31±0.04) thicknesses were the largest, 93.1±11.1 nm and comprised ~80% of the total film thickness. Additionally, partial penetration of *d*PEO within H-stack was observed for this system (f_d^H = 0.13±0.09). The greater thickness and concentration of *d*PEO in the D-stack reflect deeper penetration and a larger amount of *d*PEO absorbed by P3HMA/PEO in comparison to P3HAA/PEO. Interestingly, SLD profiles measured during these experiments did not show significant differences when the time of contact of films with *d*PEO solution was varied between 1 and 10 min, suggesting fast, sub-minute-scale infusion. This result is in stark contrast with our earlier findings for electrostatic systems, where evolution of the film SLD profiles was observed for tens of minutes during uptake of a deuterated polycation, yielding diffusion coefficients on the order of 10^{-14} cm^2/s.[57] These differences can be understood by the more dynamic nature of hydrogen bonds as compared to electrostatic pairing, and by an intrinsically high mobility of flexible PEO chains. Here, for the most diffusive P3HMA/PEO system, the lower bound of the diffusion coefficient for a 1-min uptake rate of *d*PEO within hydrogenated films of ~1×10^{-12} cm^2/s was estimated assuming the simplest case of Fickian diffusion. The fast kinetics of PEO uptake is consistent with the timescale of PEO uptake by P3HMA/PEO films measured by *in situ* ellipsometry and shown in Figure 2A. At the same time, the diffusion coefficient for *d*PEO uptake derived from neutron reflectometry is almost two orders of magnitude larger than that the upper limit estimated for the uptake of P3HMA chains seen with *in situ* ellipsometry in Figure 2B. Note that the molecular weight of *d*PEO was about 2.5 times larger than that of P3HMA. These data

again illustrate the asymmetric nature of the dynamics of PEO and P3HMA chains in exponential hydrogen-bonded films.

While neutron reflectometry probed the mobility of PEO chains within the film in the direction perpendicular to the substrate, the measurements did not track mobility of hydrogenated *l*PPh chains and does not allow one to follow mass transfer in the direction parallel to the substrate. To explore mass transfer of both *l*PPh and PEO chains and to evaluate the ability of films to heal, we applied *in situ* atomic force microscopy (AFM) and designed experiments to explore self-healing properties of *l*PPh/PEO films. This technique has previously been used to study self-healing properties in non-LbL polymer films.[63-65] Here, we scratch a film using an AFM tip and then monitor healing as a function of time. In a typical experiment, an *l*PPh/PEO film of dry thickness 400 nm was immersed in DI water, and its surface morphology was analyzed by a Bruker Dimension Icon AFM instrument using a ScanAsyst Fluid+ tip. The film surface was then pressed by the tip in contact mode with a force of 2-20 nN for 5 min. The damaged spot was subsequently scanned continuously in ScanAsyst mode using the same tip while the film was continuously immersed in water. Note that the hydrogen bonded films did not self-heal in the dry state.

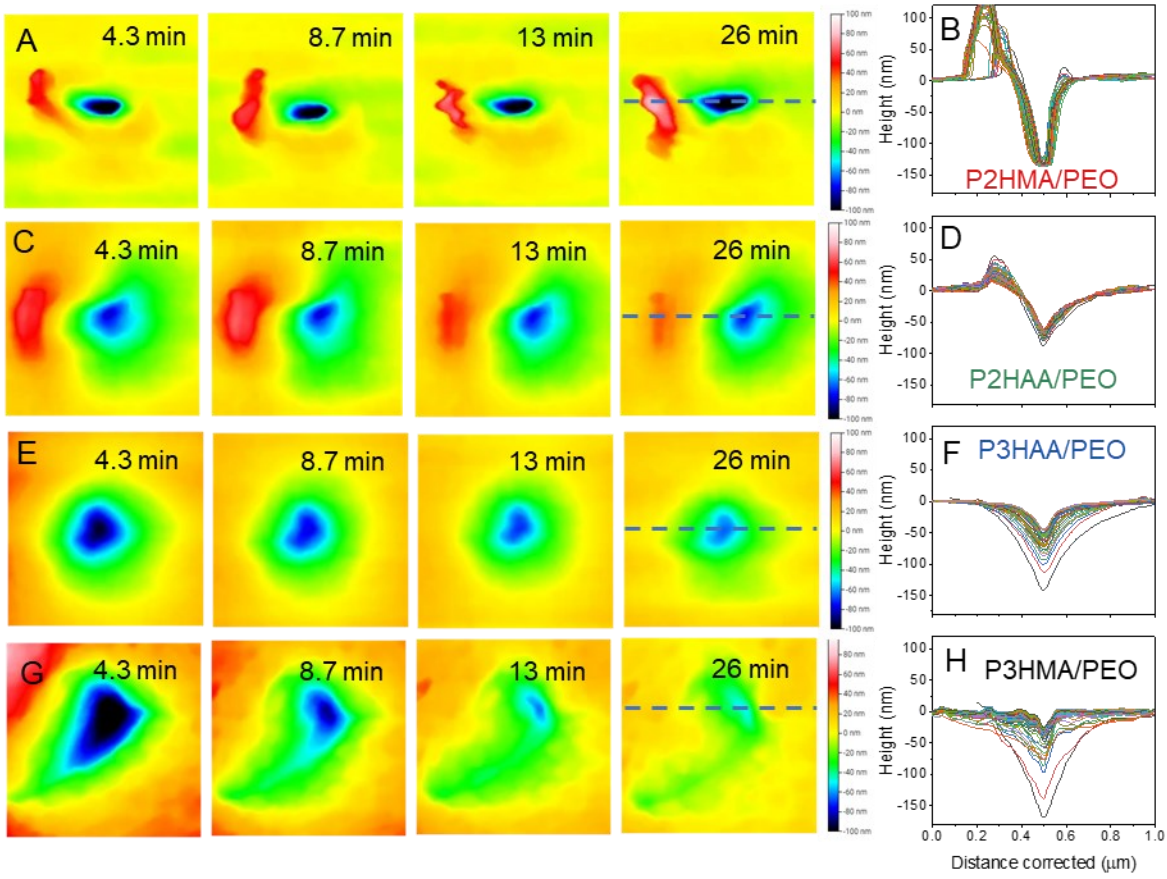

Figure 4. Self-healing of ~400-nm-thick *l*PPh/PEO films measured by *in situ* AFM during immersion in water. AFM images and depth profiles of the indented areas as a function of time for P2HMA/PEO (A, B), P2HAA/PEO (C, D), P3HAA/PEO (E, F), and P3HMA/PEO (G, H) films, respectively.

Figure 4 shows *in situ* AFM images of the time evolution of depth profiles of the damaged areas as a function of time in water after indentation. Figure 4 A, B illustrate that for P2HMA/PEO films, the area scans and depth profiles did not change with time, maintaining a pit depth of ~140 nm at the deepest point. These data show that the film built with catechol-like P2HMA did not exhibit self-healing properties. Another *l*PPh/PEO film also composed of a catechol-like

polymer but with an acrylate rather than methacrylate backbone, *i.e.* P2HAA/PEO, exhibited negligible change in the indented area (Figure 4 C, D). Self-healing in films built with gallol-like polyphenols was much more pronounced. Specifically, the P3HAA/PEO system (Figure 4 E, F) showed continuous time evolution of both the indented area and the depth profile indicating significant material flow. The P3HMA/PEO film exhibited superior self-healing and the fastest flow among all the *l*PPh/PEO systems (Figure 4 G, H). The rate of self-healing is related to mass transport of the hydrogen-bonded polymer material from the bulk of the film into the void region. The time-resolved AFM data in Figure 4 allowed us to assess the rate of mass transport in the directions parallel and perpendicular to the substrate. However, because of the uncertainties associated with the specific shape of the indented area, and the absence of an analytical solution of the Fickian diffusion equation for volumes of arbitrary shape, we were unable to determine coefficients for the mass transfer, so we instead evaluate healing through half-recovery times.

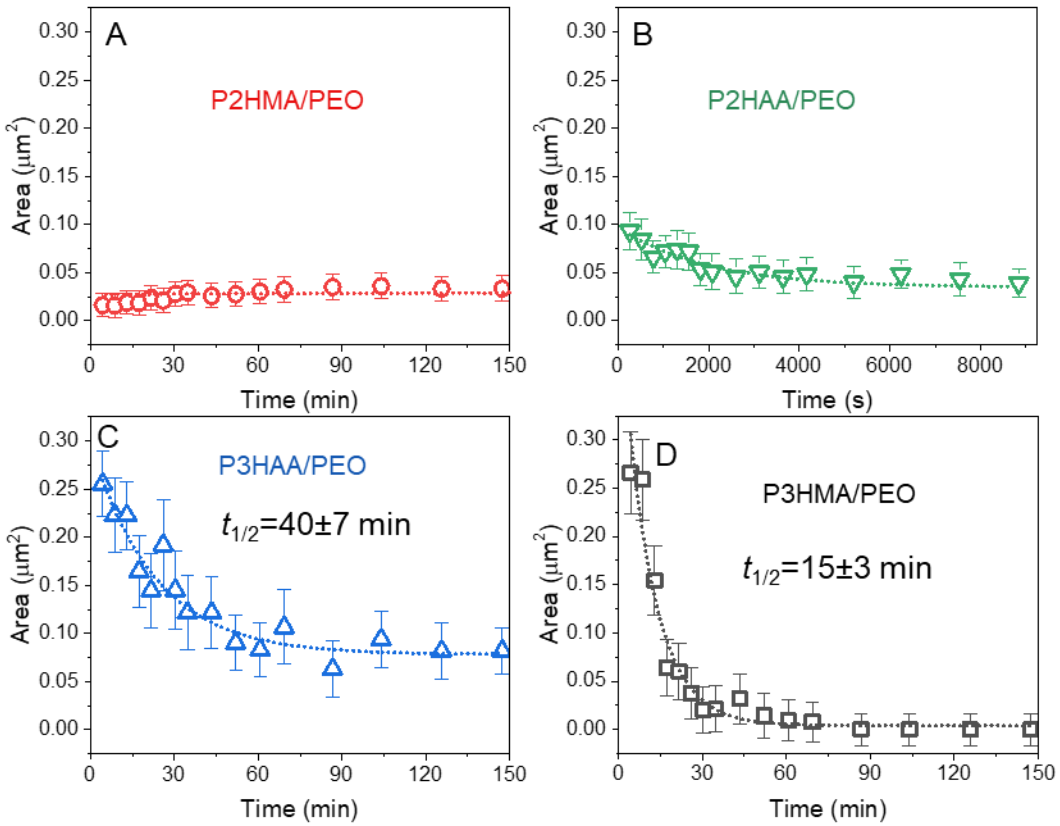

Figure 5. Time evolution of the lateral dimensions of the indented areas measured at a depth of 40 nm within the films using *in situ* AFM for P2HMA/PEO (A), P2HAA/PEO (B), P3HAA/PEO (C), and P3HMA/PEO (D) films during their continuous immersion in water.

The movement of *l*PPh/PEO in the direction parallel to the substrate was evaluated from the time evolution of the cross-section of the indented areas at a depth of 40 nm from the film surface. This choice was made to avoid the surface itself, which has been demonstrated to have faster movement of polymer chains than the 'bulk' of the film[29,33,47] and to allow uniform comparison between different *l*PPh/PEO systems by eliminating any possible effect of surface roughness on the estimated values. Figure 5A shows that with P2HMA/PEO films, the cross-

sectional area did not decrease with time. Instead, a slight increase in the size of the indented area was observed, possibly due to tip-induced effects caused by repeated scanning. This result is consistent with a complete absence of diffusivity in this system over >150 min of observation. Films of the other catechol-like polyphenol with an acrylate backbone (P2HAA) (Figure 5B) showed only a modest decrease, which was not, however, quantified here because of the negligible changes observed in depth profile that can be explained by the uncertainty associated with the selection of the surface reference line**,** which could be significantly altered by the indentation tip (Figure 4D). P3HAA/PEO films exhibited faster healing, showing a more pronounced change in the cross-sectional area from 0.26 μm^2 to 0.08 μm^2 after 150 min. Finally, the fastest dynamics and healing was observed for P3HMA/PEO films which demonstrated complete healing after a 30-min immersion in water. The half-times of recovery in the lateral direction can be estimated as 40±7 min and 15±3 min for P3HAA/PEO and P3HMA/PEO, respectively. Evaluation of lateral mobility at depths of 60 and 25 nm provided similar values of half-recovery time for all /PPh/PEO films (Figures S22, S23), indicating that the depth of measurement of the cross-sectional area did not have a significant effect on the measurements of lateral mobility.

The results in Figure 4 can also be used to evaluate diffusivity in the direction perpendicular to the substrate. Figure 6 shows the time evolution of the depth of the indented pit. Similar to results observed in the lateral direction, P2HMA/PEO and P2HAA/PEO films did not exhibit any significant mass transfer in the perpendicular direction, suggesting that, if present, dynamics was slower than the observation time (Figure 6 A, B). Again, gallol-containing films (Figure 6 C, D) exhibited robust self-healing behavior, with estimated half-recovery times of 60±7 min and 20±3 min, respectively for P3HAA/PEO and P3HMA/PEO.

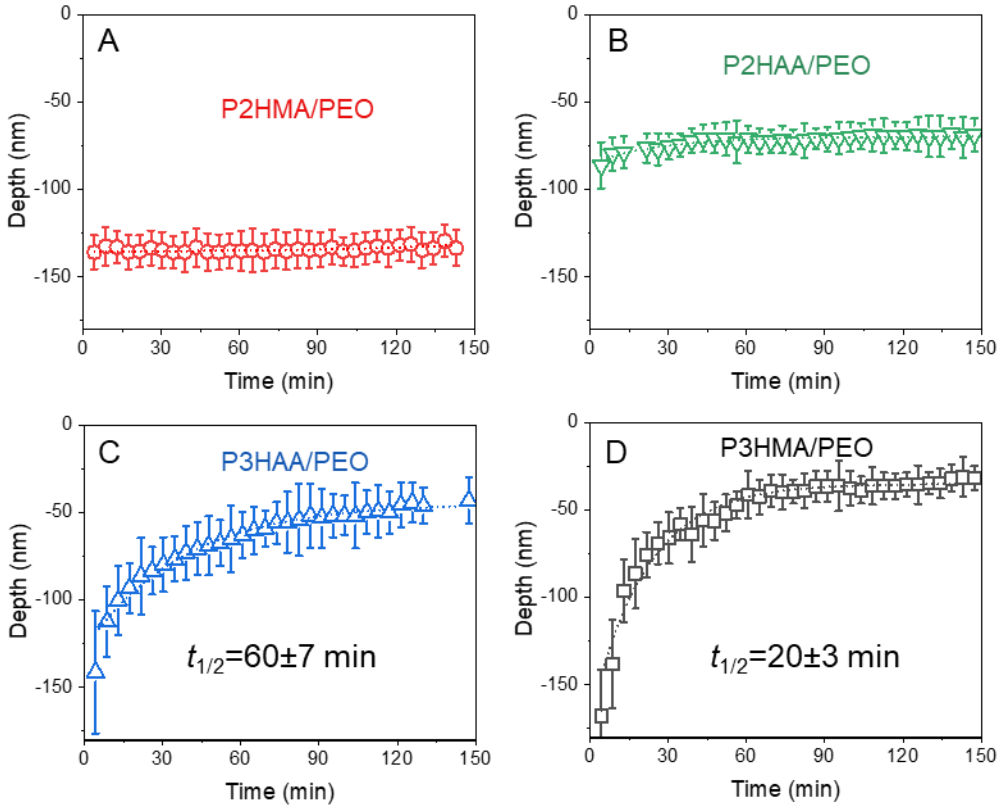

Figure 6. Time evolution of the deepest point of the indented areas measured using *in situ* AFM for P2HMA/PEO (A), P2HAA/PEO (B), P3HAA/PEO (C), and P3HMA/PEO (D) films during their continuous immersion in water.

The absence of mass transfer into the void area in both lateral and perpendicular directions for the most linear-growth-mode *l*PPh/PEO systems, *i.e.*, P2HMA/PEO and P2HAA/PEO (Figure 1) is consistent with the lack of penetration of PEO into the bulk of the film detected in the neutron reflectometry experiments (Figure 3). For films built with gallol-like polyphenols (*i.e.,* P3HAA/PEO and P3HMA/PEO films), much faster mass transfer occurred indicating a drastic enhancement of intermixing. These data are also consistent with our earlier study of the antioxidant activity of P2HMA/PEO and P3HMA/PEO films, which demonstrated significant differences in

the depth of penetration of radical species into LbL films.[53] Because polyphenol components comprised 70-80% of the mass of the exponential P3HAA/PEO and P3HMA/PEO films, measurements of film dynamics and self-healing using AFM were more sensitive to diffusion of the polyphenol components, while neutron reflectometry experiments were selective to the mobility of the minority *d*PEO component in the films. Assessment of the characteristic time scales for self-healing of P3/PEO films suggests that mass transfer in these films is likely isotropic parallel and perpendicular to the substrate, despite the surface-supported, layer-by-layer film deposition. Our finding of low anisotropy of diffusion in *l*PPh/PEO hydrogen-bonded systems contrasts with the large anisotropy earlier reported in polyelectrolyte multilayer systems. For example, 10^4–10^5 faster polymer chain diffusion was found for poly(2-(dimethylamino)ethyl methacrylate) – poly(methacrylic acid) films exposed to NaCl solutions.[47] Weaker stratification of hydrogen-bonded LbL films is generally seen than in electrostatic systems, and it frequently decays with distance from the substrate.[38,46] Note that direct measurements of the degree of film stratification for films thicker than about 300 nm (such as those studied by AFM in this work) cannot be performed by neutron reflectometry, and that a decay of film stratification with distance from the substrate can contribute to a lack of anisotropy in mass transfer in hydrogen-bonded films. Overall weaker interpolymer interactions in hydrogen-bonded films can also account for this difference, although the lack of healing in P2/PEO films is not consistent with this explanation. The presence of electrostatic pairing, electrostatic barriers to layer intermixing, and local charge control of ionic pair rearrangements in electrostatic systems may be responsible for the significant differences seen in the structure and dynamics of electrostatic and hydrogen bonded LbL films.

In conclusion, we have shown that the structure of polyphenol rings can strongly affect the dynamics of hydrogen-bonded films and have evaluated mass movement using *in situ*

ellipsometry, neutron reflectometry and *in situ* AFM. A wide range of behavior, varying from non-diffusive at the experimental time scale to fast self-healing upon exposure to aqueous solutions was seen for LbL films of polyphenols with different polyphenol repeat units. An interesting finding was the distinctly different chain dynamics in P3/PEO assemblies featuring the gallol polyphenol ring structure, which demonstrated fast binding of flexible PEO chains at the surface of the film, or fast penetration of PEO throughout the entire LbL film for acryl or methacryl polymer backbones, respectively. In contrast to the fast diffusion of PEO chains, dynamics of film mass transfer during self-healing correlated with a much slower diffusion of P3 chains measured by *in situ* ellipsometry, suggesting that diffusion of P3 chains limits the transport of associated P3/PEO chains within hydrogen-bonded films. However, more flexible PEO can achieve faster diffusion by exchange with bound PEO in the film. Because of the significant antioxidant activity of *l*PPh/PEO assemblies, experiments reported in this work can help to rationally construct functional coatings with both antioxidant and self-healing ability. Moreover, small-molecule competitors can be used in future work to regulate hydrogen bonding[36] and the self-healing behavior of these films.

Supporting Information

Synthetic procedure and GPC characterization for P2HAA and P3HAA, neutron scattering data, fitting models and parameters of neutron reflectivity studies, and *in situ* AFM data.

This material is available free of charge via the Internet at http://pubs.acs.org.

Corresponding Author

*E-mail: svetlana@tamu.edu.

Notes

The authors declare no competing financial interest.

Acknowledgment

This work was supported by the National Science Foundation under Award DMR-1905535 (S.S.). Neutron measurements were performed at the Spallation Neutron Source at the Oak Ridge National Laboratory, managed by UT-Battelle, LLC, for the DOE under contract No. DE-AC05-00OR. *Use of the TAMU Materials Characterization Facility is acknowledged.* The authors thank Hanna Hlushko for help with TOC image preparation.

References

(1) Shukla, A.; Almeida, B. Advances in cellular and tissue engineering using layer-by-layer assembly. *WIREs Nanomedicine and Nanobiotechnology* **2014**, *6*, 411-421.

(2) Gentile, P.; Ferreira, A. M.; Callaghan, J. T.; Miller, C. A.; Atkinson, J.; Freeman, C.; Hatton, P. V. Multilayer Nanoscale Encapsulation of Biofunctional Peptides to Enhance Bone Tissue Regeneration In Vivo. *Advanced Healthcare Materials* **2017**, *6*, 1601182.

(3) Gentile, P.; Ghione, C.; Ferreira, A. M.; Crawford, A.; Hatton, P. V. Alginate-based hydrogels functionalised at the nanoscale using layer-by-layer assembly for potential cartilage repair. *Biomaterials Science* **2017**, *5*, 1922-1931.

(4) Pavlukhina, S.; Sukhishvili, S. Polymer assemblies for controlled delivery of bioactive molecules from surfaces. *Advanced Drug Delivery Reviews* **2011**, *63*, 822-836.

(5) Liu, X.; Han, F.; Zhao, P.; Lin, C.; Wen, X.; Ye, X. Layer-by-layer self-assembled multilayers on PEEK implants improve osseointegration in an osteoporosis rabbit model. *Nanomedicine: Nanotechnology, Biology and Medicine* **2017**, *13*, 1423-1433.

(6) Schoeler, B.; Kumaraswamy, G.; Caruso, F. Investigation of the Influence of Polyelectrolyte Charge Density on the Growth of Multilayer Thin Films Prepared by the Layer-by-Layer Technique. *Macromolecules* **2002**, *35*, 889-897.

(7) Decher, G.; Hong, J. D.; Schmitt, J. Buildup of ultrathin multilayer films by a self-assembly process: III. Consecutively alternating adsorption of anionic and cationic polyelectrolytes on charged surfaces. *Thin Solid Films* **1992**, *210-211*, 831-835.

(8) Decher, G. Fuzzy Nanoassemblies: Toward Layered Polymeric Multicomposites. *Science* **1997**, *277*, 1232-1237.

(9) Liljeström, V.; Ora, A.; Hassinen, J.; Rekola, H. T.; Nonappa; Heilala, M.; Hynninen, V.; Joensuu, J. J.; Ras, R. H. A.; Törmä, P.; Ikkala, O.; Kostiainen, M. A. Cooperative colloidal self-assembly of metal-protein superlattice wires. *Nature communications* **2017**, *8*, 671.

(10) Kotov, N. A. Layer-by-layer self-assembly: The contribution of hydrophobic interactions. *Nanostructured Materials* **1999**, *12*, 789-796.

(11) Kharlampieva, E.; Kozlovskaya, V.; Sukhishvili, S. A. Layer-by-Layer Hydrogen-Bonded Polymer Films: From Fundamentals to Applications. *Advanced Materials* **2009**, *21*, 3053-3065.

(12) Borges, J.; Mano, J. F. Molecular Interactions Driving the Layer-by-Layer Assembly of Multilayers. *Chemical Reviews* **2014**, *114*, 8883-8942.

(13) Quinn, J. F.; Johnston, A. P. R.; Such, G. K.; Zelikin, A. N.; Caruso, F. Next generation, sequentially assembled ultrathin films: beyond electrostatics. *Chemical Society Reviews* **2007**, *36*, 707-718.

(14) Stockton, W. B.; Rubner, M. F. Molecular-Level Processing of Conjugated Polymers. 4. Layer-by-Layer Manipulation of Polyaniline via Hydrogen-Bonding Interactions. *Macromolecules* **1997**, *30*, 2717-2725.

(15) Wang, L.; Wang, Z.; Zhang, X.; Shen, J.; Chi, L.; Fuchs, H. A new approach for the fabrication of an alternating multilayer film of poly(4-vinylpyridine) and poly(acrylic acid) based on hydrogen bonding. *Macromolecular Rapid Communications* **1997**, *18*, 509-514.

(16) Kozlovskaya, V.; Ok, S.; Sousa, A.; Libera, M.; Sukhishvili, S. A. Hydrogen-Bonded Polymer Capsules Formed by Layer-by-Layer Self-Assembly. *Macromolecules* **2003**, *36*, 8590-8592.

(17) Sukhishvili, S. A.; Granick, S. Layered, Erasable Polymer Multilayers Formed by Hydrogen-Bonded Sequential Self-Assembly. *Macromolecules* **2002**, *35*, 301-310.

(18) Quinn, J. F.; Caruso, F. Facile Tailoring of Film Morphology and Release Properties Using Layer-by-Layer Assembly of Thermoresponsive Materials. *Langmuir* **2004**, *20*, 20-22.

(19) DeLongchamp, D. M.; Hammond, P. T. Highly Ion Conductive Poly(ethylene oxide)-Based Solid Polymer Electrolytes from Hydrogen Bonding Layer-by-Layer Assembly. *Langmuir* **2004**, *20*, 5403-5411.

(20) Erel-Unal, I.; Sukhishvili, S. A. Hydrogen-Bonded Multilayers of a Neutral Polymer and a Polyphenol. *Macromolecules* **2008**, *41*, 3962-3970.

(21) Kozlovskaya, V.; Harbaugh, S.; Drachuk, I.; Shchepelina, O.; Kelley-Loughnane, N.; Stone, M.; Tsukruk, V. V. Hydrogen-bonded LbL shells for living cell surface engineering. *Soft Matter* **2011**, *7*, 2364-2372.

(22) Kozlovskaya, V.; Kharlampieva, E.; Drachuk, I.; Cheng, D.; Tsukruk, V. V. Responsive microcapsule reactors based on hydrogen-bonded tannic acid layer-by-layer assemblies. *Soft Matter* **2010**, *6*, 3596-3608.

(23) Kozlovskaya, V.; Wang, Y.; Higgins, W.; Chen, J.; Chen, Y.; Kharlampieva, E. pH-triggered shape response of cubical ultrathin hydrogel capsules. *Soft Matter* **2012**, *8*, 9828-9839.

(24) Liu, F.; Kozlovskaya, V.; Zavgorodnya, O.; Martinez-Lopez, C.; Catledge, S.; Kharlampieva, E. Encapsulation of anticancer drug by hydrogen-bonded multilayers of tannic acid. *Soft Matter* **2014**, *10*, 9237-9247.

(25) Pham-Hua, D.; Padgett, L. E.; Xue, B.; Anderson, B.; Zeiger, M.; Barra, J. M.; Bethea, M.; Hunter, C. S.; Kozlovskaya, V.; Kharlampieva, E.; Tse, H. M. Islet encapsulation with polyphenol coatings decreases pro-inflammatory chemokine synthesis and T cell trafficking. *Biomaterials* **2017**, *128*, 19-32.

(26) Decher, G.: Layer-by-Layer Assembly (Putting Molecules to Work). In *Multilayer Thin Films*; pp 1-21.

(27) Elbert, D. L.; Herbert, C. B.; Hubbell, J. A. Thin Polymer Layers Formed by Polyelectrolyte Multilayer Techniques on Biological Surfaces. *Langmuir* **1999**, *15*, 5355-5362.

(28) Ruths, J.; Essler, F.; Decher, G.; Riegler, H. Polyelectrolytes I: Polyanion/Polycation Multilayers at the Air/Monolayer/Water Interface as Elements for Quantitative Polymer Adsorption Studies and Preparation of Hetero-superlattices on Solid Surfaces. *Langmuir* **2000**, *16*, 8871-8878.

(29) Xu, L.; Selin, V.; Zhuk, A.; Ankner, J. F.; Sukhishvili, S. A. Molecular Weight Dependence of Polymer Chain Mobility within Multilayer Films. *ACS Macro Letters* **2013**, *2*, 865-868.

(30) Jang, Y.; Seo, J.; Akgun, B.; Satija, S.; Char, K. Molecular Weight Dependence on the Disintegration of Spin-Assisted Weak Polyelectrolyte Multilayer Films. *Macromolecules* **2013**, *46*, 4580-4588.

(31) Nazaran, P.; Bosio, V.; Jaeger, W.; Anghel, D. F.; v. Klitzing, R. Lateral Mobility of Polyelectrolyte Chains in Multilayers. *The Journal of Physical Chemistry B* **2007**, *111*, 8572-8581.

(32) Kharlampieva, E.; Ankner, J. F.; Rubinstein, M.; Sukhishvili, S. A. $p\mathrm{H}$-Induced Release of Polyanions from Multilayer Films. *Physical Review Letters* **2008**, *100*, 128303.

(33) Selin, V.; Ankner, J. F.; Sukhishvili, S. A. Diffusional Response of Layer-by-Layer Assembled Polyelectrolyte Chains to Salt Annealing. *Macromolecules* **2015**, *48*, 3983-3990.

(34) Wong, J. E.; Zastrow, H.; Jaeger, W.; von Klitzing, R. Specific Ion versus Electrostatic Effects on the Construction of Polyelectrolyte Multilayers. *Langmuir* **2009**, *25*, 14061-14070.

(35) Selin, V.; Ankner, J. F.; Sukhishvili, S. A. Ionically Paired Layer-by-Layer Hydrogels: Water and Polyelectrolyte Uptake Controlled by Deposition Time. *Gels* **2018**, *4*.

(36) Selin, V.; Aliakseyeu, A.; Ankner, J. F.; Sukhishvili, S. A. Effect of a Competitive Solvent on Binding Enthalpy and Chain Intermixing in Hydrogen-Bonded Layer-by-Layer Films. *Macromolecules* **2019**, *52*, 4432-4440.

(37) Kharlampieva, E.; Sukhishvili, S. A. Hydrogen-Bonded Layer-by-Layer Polymer Films. *Journal of Macromolecular Science, Part C* **2006**, *46*, 377-395.

(38) Kharlampieva, E.; Kozlovskaya, V.; Ankner, J. F.; Sukhishvili, S. A. Hydrogen-Bonded Polymer Multilayers Probed by Neutron Reflectivity. *Langmuir* **2008**, *24*, 11346-11349.

(39) Guan, Y.; Zhang, Y. Dynamically bonded layer-by-layer films: Dynamic properties and applications. *Journal of Applied Polymer Science* **2014**, *131*.

(40) Zhao, Y.-N.; Gu, J.; Jia, S.; Guan, Y.; Zhang, Y. Zero-order release of polyphenolic drugs from dynamic, hydrogen-bonded LBL films. *Soft Matter* **2016**, *12*, 1085-1092.

(41) Grdadolnik, J.; Merzel, F.; Avbelj, F. Origin of hydrophobicity and enhanced water hydrogen bond strength near purely hydrophobic solutes. *Proceedings of the National Academy of Sciences* **2017**, *114*, 322.

(42) Zhuk, A.; Selin, V.; Zhuk, I.; Belov, B.; Ankner, J. F.; Sukhishvili, S. A. Chain Conformation and Dynamics in Spin-Assisted Weak Polyelectrolyte Multilayers. *Langmuir* **2015**, *31*, 3889-3896.

(43) Fortier-McGill, B.; Reven, L. 2H NMR Studies of Polymer Multilayer Capsules, Films, and Complexes. *Macromolecules* **2009**, *42*, 247-254.

(44) Soltwedel, O.; Ivanova, O.; Nestler, P.; Müller, M.; Köhler, R.; Helm, C. A. Interdiffusion in Polyelectrolyte Multilayers. *Macromolecules* **2010**, *43*, 7288-7293.

(45) Jomaa, H. W.; Schlenoff, J. B. Salt-Induced Polyelectrolyte Interdiffusion in Multilayered Films: A Neutron Reflectivity Study. *Macromolecules* **2005**, *38*, 8473-8480.

(46) Xu, L.; Ankner, J. F.; Sukhishvili, S. A. Steric Effects in Ionic Pairing and Polyelectrolyte Interdiffusion within Multilayered Films: A Neutron Reflectometry Study. *Macromolecules* **2011**, *44*, 6518-6524.

(47) Xu, L.; Kozlovskaya, V.; Kharlampieva, E.; Ankner, J. F.; Sukhishvili, S. A. Anisotropic Diffusion of Polyelectrolyte Chains within Multilayer Films. *ACS Macro Letters* **2012**, *1*, 127-130.

(48) Dubas, S. T.; Schlenoff, J. B. Swelling and Smoothing of Polyelectrolyte Multilayers by Salt. *Langmuir* **2001**, *17*, 7725-7727.

(49) Ghostine, R. A.; Jisr, R. M.; Lehaf, A.; Schlenoff, J. B. Roughness and Salt Annealing in a Polyelectrolyte Multilayer. *Langmuir* **2013**, *29*, 11742-11750.

(50) Fortier-McGill, B.; Toader, V.; Reven, L. Chain Dynamics of Water-Saturated Hydrogen-Bonded Polymer Complexes and Multilayers. *Macromolecules* **2011**, *44*, 2755-2765.

(51) Hlushko, H.; Cubides, Y.; Hlushko, R.; Kelly, T. M.; Castaneda, H.; Sukhishvili, S. A. Hydrophobic Antioxidant Polymers for Corrosion Protection of an Aluminum Alloy. *ACS Sustainable Chemistry & Engineering* **2018**, *6*, 14302-14313.

(52) Hlushko, R.; Hlushko, H.; Sukhishvili, S. A. A family of linear phenolic polymers with controlled hydrophobicity, adsorption and antioxidant properties. *Polymer Chemistry* **2018**, *9*, 506-516.

(53) Hlushko, R.; Ankner, J. F.; Sukhishvili, S. A. Layer-by-Layer Hydrogen-Bonded Antioxidant Films of Linear Synthetic Polyphenols. *Macromolecules* **2020**, *53*, 1033-1042.

(54) Dubas, S. T.; Schlenoff, J. B. Factors controlling the growth of polyelectrolyte multilayers. *Macromolecules* **1999**, *32*, 8153-8160.

(55) Woollam, J. A.; Johs, B. D.; Herzinger, C. M.; Hilfiker, J. N.; Synowicki, R. A.; Bungay, C. L.: *Overview of variable-angle spectroscopic ellipsometry (VASE): I. Basic theory and typical applications*; SPIE, 1999; Vol. 10294. pp. OP.

(56) Al-Faleh, R. S.; Zihlif, A. M. A study on optical absorption and constants of doped poly(ethylene oxide). *Physica B: Condensed Matter* **2011**, *406*, 1919-1925.

(57) Selin, V.; Ankner, J. F.; Sukhishvili, S. A. Nonlinear Layer-by-Layer Films: Effects of Chain Diffusivity on Film Structure and Swelling. *Macromolecules* **2017**, *50*, 6192-6201.

(58) Metzler, R.; Klafter, J. The random walk's guide to anomalous diffusion: a fractional dynamics approach. *Physics Reports* **2000**, *339*, 1-77.

(59) Metzler, R.; Jeon, J.-H.; Cherstvy, A. G.; Barkai, E. Anomalous diffusion models and their properties: non-stationarity, non-ergodicity, and ageing at the centenary of single particle tracking. *Physical Chemistry Chemical Physics* **2014**, *16*, 24128-24164.

(60) Bouchaud, J.-P.; Georges, A. Anomalous diffusion in disordered media: Statistical mechanisms, models and physical applications. *Physics Reports* **1990**, *195*, 127-293.

(61) Kienle, D. F.; Schwartz, D. K. Complex Salt Dependence of Polymer Diffusion in Polyelectrolyte Multilayers. *The Journal of Physical Chemistry Letters* **2019**, *10*, 987-992.

(62) Pethe, V. V.; Wang, H. P.; Hiltner, A.; Baer, E.; Freeman, B. D. Oxygen and carbon dioxide permeability of EAA/PEO blends and microlayers. *Journal of Applied Polymer Science* **2008**, *110*, 1411-1419.

(63) South, A. B.; Lyon, L. A. Autonomic Self-Healing of Hydrogel Thin Films. *Angewandte Chemie International Edition* **2010**, *49*, 767-771.

(64) Kratz, K.; Narasimhan, A.; Tangirala, R.; Moon, S.; Revanur, R.; Kundu, S.; Kim, H. S.; Crosby, A. J.; Russell, T. P.; Emrick, T.; Kolmakov, G.; Balazs, A. C. Probing and repairing damaged surfaces with nanoparticle-containing microcapsules. *Nature Nanotechnology* **2012**, *7*, 87-90.

(65) Yoon, J. A.; Kamada, J.; Koynov, K.; Mohin, J.; Nicolaÿ, R.; Zhang, Y.; Balazs, A. C.; Kowalewski, T.; Matyjaszewski, K. Self-Healing Polymer Films Based on Thiol–Disulfide Exchange Reactions and Self-Healing Kinetics Measured Using Atomic Force Microscopy. *Macromolecules* **2012**, *45*, 142-149.

For Table of Contents Only

Dynamics and Self-Healing of Layer-by-Layer Hydrogen-Bonded Films of Linear Synthetic Polyphenols

Raman Hlushko[1], John F. Ankner[2], and Svetlana Sukhishvili[1]*

[1]*Department of Materials Science and Engineering, Texas A&M University*

College Station, Texas 77843, USA

[2]*Spallation Neutron Source, Oak Ridge National Laboratory, Oak Ridge, Tennessee 37831, USA*